Macromolecular Materials and Engineering
www.mme-journal.de

Developments in Pressurized Gyration for the Mass Production of Polymeric Fibers

*Phoebe L. Heseltine, Jubair Ahmed, and Mohan Edirisinghe**

In this invited feature article, the invention of pressurized gyration in 2013 and its subsequent development into sister processes such as pressurized melt gyration, infusion gyration, and pressure-coupled infusion gyration is elucidated. The fundamentals of these processes are discussed, elucidating how these novel methods can be used to facilitate mass production of polymeric fibers and other morphologies. The effects of the main system parameters: rotational speed and gas pressure, are discussed along with the influence of solution parameters such as viscosity and polymer chain entanglement. The effect of flow of material into the gyrator in infused gyration is also illustrated. Examples of many polymers that have been subjected to these processes are discussed and the applications of resulting products are illustrated under several different research themes such as, tissue engineering, drug delivery, diagnostics, hydrogels, filtration, and wound healing.

1. Introduction

To produce functional materials from polymeric fibers, for example, biomaterials, forming must take place on a technologically relevant scale, with a high surface area and tunable porosity.[1] Materials with these characteristics have been utilized in filtration, medical textiles, biosensing, catalysis, lab-on-chip technologies, as scaffolds in tissue engineering, and as encapsulation materials in therapeutic delivery.[2–7] Still, the demand for ultrafine polymeric fibers is on the rise due to their inherent versatility.[8] To be valuable in all of these application areas, it is critical that fibers can be mass produced in a consistent, reliable, and cost-effective manner.[9]

Nanostructured polymeric materials with the aforementioned characteristics have been produced via a number of methods. These include phase separation, template synthesis, bicomponent fiber production, self-assembly, centrifugal spinning, melt blowing, and electrospinning.[10–16] While all of these approaches have advantages, they are not without their limitations. Although nanofoams with highly desirable structures can be produced using phase separation, the process is complicated and lengthy. Additionally, while self-assembly is capable of producing very fine diameter fibers, the productivity level of this method is very low.[14] As a result, electrospinning is one of the most widespread laboratory fiber fabrication techniques and is certainly one of the most widely reported in academic literature.

Electrospinning is largely successful in that it affords fibers in the nanometer range that can be produced continuously, yet it is by no means perfect.[17] It requires high voltages to overcome the surface tension of the polymer solution in order to produce fibers which it deposits in a whipping motion, leading to random alignment due to electrostatic interactions and asymmetric instabilities.[18] Although the commercial viability is limited somewhat due to the emergence of only single fibers from the nozzle, polymide nanofibers have been scaled-up for energy storage applications.[19,20]

Nozzle-free methods of fiber production have been developed through centrifugal spinning, a voltage-free technique that relies on centrifugal force to produce fine fibers which, like electrospinning, has a wide variety of applications—from energy storage to tissue engineering.[21–24] Forcespinning, a type of centrifugal spinning, can produce nanoscale fibers through careful design of geometry and morphology of spinnerets.[25] These methods have demonstrated superior fiber yields compared to previous electric field–based methods and variations on these have been developed such as liquid shearing spinning, brush spinning, and magnetospinning.[26–29]

Established in 2013, pressurized gyration (PG) combines the features of solution blowing and centrifugal spinning to produce large quantities of homogenous fibers with even greater control over final product morphology due to the increased number of parameters that can be finely tuned.[30] At nearly 5 years since its inception, this is a timely opportunity to feature the research and development conducted using this polymer processing method and to analyze its success to date. Here, we provide a thorough introduction to PG, detailing all of the processing and solution parameters involved. The research to date is summarized and an outline of application areas and future scope is provided.

P. L. Heseltine, J. Ahmed, Prof. M. Edirisinghe
Department of Mechanical Engineering
University College London
Torrington Place, London WC1E 7JE, UK
E-mail: m.edirisinghe@ucl.ac.uk

The ORCID identification number(s) for the author(s) of this article can be found under https://doi.org/10.1002/mame.201800218.

DOI: 10.1002/mame.201800218

2. Fundamentals of Pressurized Gyration

The laboratory setup of PG (Mark I device) consists of a small (35 mm × 60 mm) aluminium cylindrical vessel with multiple, narrow (0.5 mm) perforations.[20] The vessel itself is attached to an electric motor, capable of rotational speeds of up to 36 000 rpm. Speed can be easily varied via the use of a controller that adjusts the current to the motor. A gas inlet that feeds nitrogen via plastic tubing is fastened to the lid of the vessel. The gas pressure can be increased up to 0.3 MPa. A pre-prepared polymer solution is loaded into the interior of the rotating vessel and the gas inlet is secured in position. The process of forming fibers occurs following the combined application of the motor and gas pressure. As the vessel rotates, the solution is forced out through the perforations and extrudes as a polymer jet which dries, leaving behind fibers.[31,32] The apparatus is situated within a chamber in which fibers are deposited and later collected. (**Figure 1)** summarizes the basic setup.

2.1. Principles of Pressurized Gyration

PG operates through the manipulation of the Rayleigh–Taylor instability of a chosen polymer solution. Upon starting the motor, the rotational speed rapidly increases, leading to a greater centrifugal force, causing displacement of the polymer solution. The applied gas pressure acts against the liquid causing a pressure differential in the vessel, forcing the solution out. Centrifugal force is the main driver behind liquid extrusion through the vessel orifices.[33] A focused polymer jet

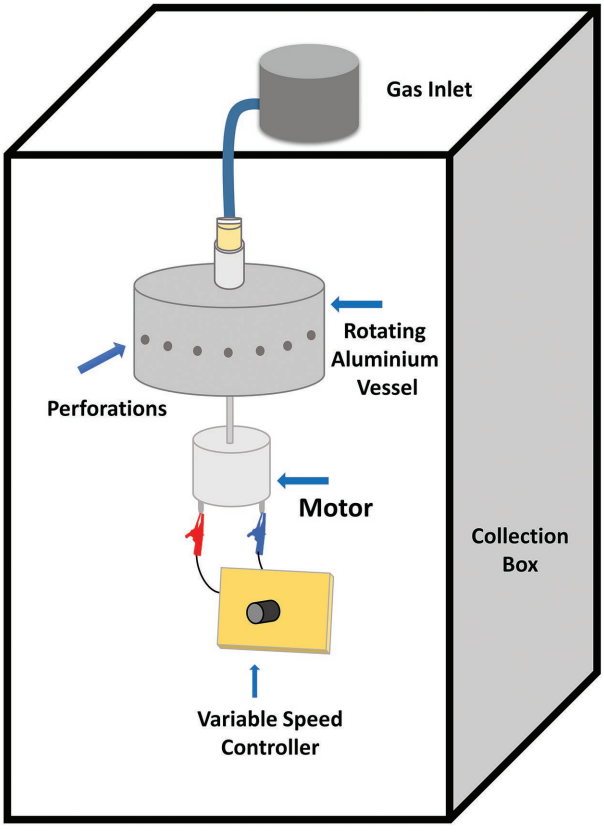

Figure 1. Schematic overview of the fundamental pressurized gyration equipment rig.

Phoebe L. Heseltine is a Ph.D. student in the Department of Mechanical Engineering at University College London. She received her B.S. in nanotechnology (chemistry) from the University of Leeds. Following an M.S. in biomaterials and tissue engineering in 2016, Phoebe joined the Biomaterials Processing Laboratory of Prof. Mohan Edirisinghe to undertake an EPSRC-BASF National Productivity Investment Fund Ph.D. Studentship. Her current research focuses on the preparation, modification, and characterization of polymeric fibers for use in healthcare devices.

Jubair Ahmed is a Ph.D. student at University College London in the Department of Mechanical Engineering. He obtained his B.S. in biochemistry from the University of Westminster. Jubair followed on to attain his M.S. in biomaterials and tissue engineering at University College London with distinction and top marks. Jubair is interested in utilizing engineering approaches to overcome major biomedical issues. Jubair's current research focuses on the novel manufacture of materials for wound dressings and other healthcare products.

Mohan Edirisinghe, was awarded a Doctor of Science degree from the University of Leeds and has held academic positions in many UK and international universities. He currently holds the Bonfield Chair of Biomaterials in the Department of Mechanical Engineering at University College London. He has led advanced materials innovative forming and manufacturing research, with healthcare applications in particular, and further details are provided on his website. He invented gyrospinning in 2013 and its development has been featured in 10 journal front covers to date.

is created as a surface tension gradient occurs along the liquid–air interface.[30] This gradient is also responsible for prompting a Marangoni stress tangential to the liquid–gas interface, which instigates flow to the tip of the polymer droplet.[34]

Formation of fibers arises when the polymer jet leaving the perforations is continually stretched by the centrifugal force and the pressure differential created by the gas inlet at the orifices.[35] The solvent is gradually lost by evaporation and the extruded polymer remaining in the jet is the origin of a fiber strand. The dried fiber is eventually deposited on the nearby collection walls; the process is rapidly repeated to give rise to a bundle of fibers.

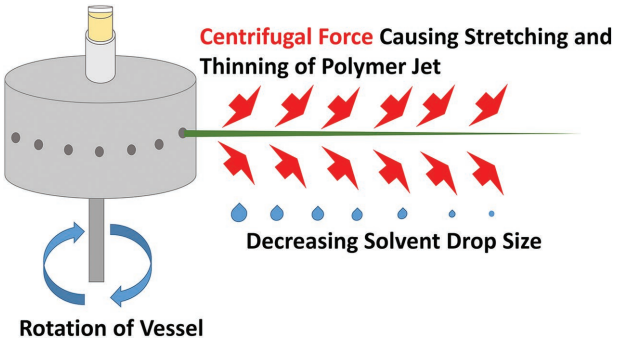

Figure 2. Diagrammatic representation of the pressurized gyration spinning process demonstrating the effect of centrifugal force on the polymer jet.

2.2. System Parameters

Fiber formation is highly dependent on the solution properties and the processing parameters. Solution properties ultimately govern spinnability and can be found to affect fiber formation just as they would in other methods such as electrospinning.[36,37] The rotational speed of the vessel and the applied gas pressure are the two most crucial processing parameters that have a marked effect on fiber morphology. Furthermore, variation of collection distance and environmental conditions alters fiber structure.

2.2.1. Rotational Speed

Centrifugal force intensifies with increasing rotational speed; therefore, higher rotational speed of the vessel results in greater manipulation of the polymer solution. The polymer jet is continually stretched and elongated by the centrifugal force and the solvent promptly evaporates, presenting fine fibers.

A critical minimum rotational speed must be met for fiber formation. Below this, the centrifugal force cannot overcome the surface tension and there is no polymer jet. At low rotational speeds and as the vessel is accelerating, the solvent may separate from the polymer due to its lower surface tension. Typically, a polymer jet does not form in this scenario and solvent is lost to the surrounding collection walls. As such, a suitable rotational speed is essential for the production of a polymer jet and subsequent fiber formation.

The solution properties, mainly surface tension, influence the minimum critical rotational speed. Beyond the threshold speed, subsequent increases in rotational speeds will cause even greater stretching and thinning of the polymer jet. Rapid solvent evaporation occurs as the surface area is increased and this results in smaller diameter fibers (**Figure 2**). The implications of even higher rotational speeds on polymer jet stability are yet to be explored.

2.2.2. Gas Pressure

For optimal fiber yield and morphology, gas pressure must be applied after reaching critical rotational speed. During the initial acceleration phase of the motor, critical rotational speed is not met and the application of gas pressure causes loss of solvent through the orifices, as the solvent has a lower surface tension than the polymer. This is because, the gas pressure acts as the driving force and the solution is expelled through the vessel apertures whilst having insufficient pressure differential to overcome the surface tension to form a polymer jet. The higher the gas pressure the greater the loss of solvent.

Fiber morphology is directly influenced by applied gas pressure. A pressure differential within the vessel causes acceleration of the solution through the orifices.[38] The gas pressure contributes to additional polymer jet elongation by way of fluid acceleration and increased kinetic energy of the emerging jet. Jet elongation yields lower diameter fibers as the polymer jet lengthens, leading to rapid solvent evaporation.[39] Although a maximum of 0.3 MPa applied pressure is generally used, the effects of even higher pressures are yet to be investigated.

Surface topography of the formed fibers can be altered by varying gas pressure. When highly volatile solvents are used, this causes a local temperature drop and surface pores result due to water droplet evaporation from the fiber surface.[40] At higher applied working pressures, the temperature drop is greater, leading to more rapid solvent evaporation and pore formation.

2.2.3. Collection Setup

Manipulation of collection distance gives rise to bead-on-string morphology, which can be advantageous in producing superhydrophobic fibers with good mechanical integrity—both excellent properties for air filtration applications.[41,42] The formation of bead-on-string fibers can be controlled by solution molecular weight and concentration.[43] At shorter collection distances, solvent evaporation is reduced and solvent droplets remain on the fiber chain. These unevaporated droplets prevent proper mixing of the polymer within the drying jet, creating beaded fibers.

Fiber diameter is reduced by increased collection distances. The jet is allowed to stretch further at higher distances, leading to narrower fibers (Figure 2). Jet thinning coupled with increased solvent evaporation leads to thinner fibers on the collector. With insufficient collection distance the motion of the jet is obstructed and fiber morphology is altered.

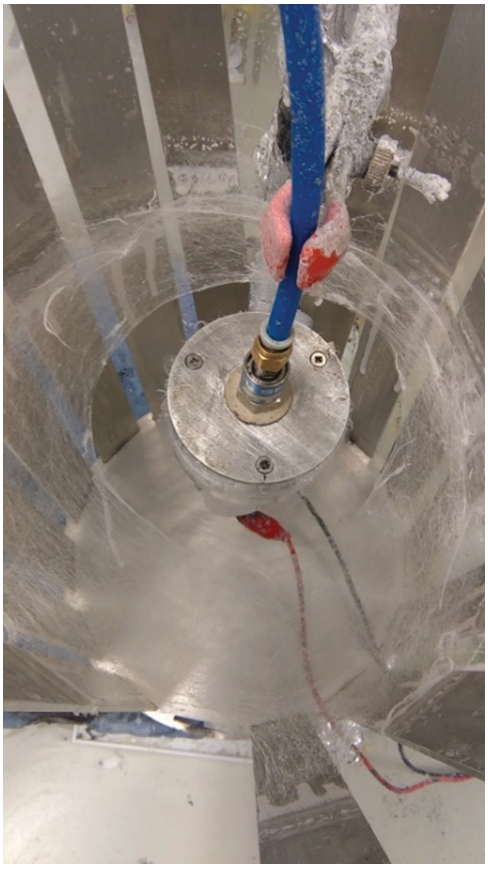

Figure 3. Collection setup that has produced highly aligned fibers.

Various modifications to the collectors have been used to influence fiber morphology and deposition. By incorporating a collector similar to that in **Figure 3**, uniaxially aligned fibers can be achieved. The collection setup increases fiber alignment due to the placement of protruding rods oriented around the pot.

2.3. Infusion Gyration

Infusion gyration is a novel technique based on PG that allows for the regulation of solution flow rate, which can directly influence yield, fiber size, distribution, and morphology. This setup overcomes the limitations in the lack of control over the flow dynamics of the polymer solution from the Mark I device. The setup comprises an aluminium cylindrical vessel with 20 small perforations on its face. The bottom of the vessel is fastened to a high-speed motor which allows the vessel to rotate at speeds of up to 36 000 rpm. The gas pressure inlet is replaced with an inlet joined to a syringe pump, allowing for solution flow-rate control.

Infusion gyration is dependent on the polymer infusion rate rather than the gas flow. The precise control over the flow rate allows for the fabrication of well-aligned, smooth, and bead-free nanofibers.[44] At higher flow rates, there is an increase in hydrostatic pressure. At the orifice, the hydrostatic pressure is lower than the centrifugal force and thus the final fiber size and distribution is determined by the destabilizing centrifugal force and the surface tension of the polymer solution.[45] Fiber diameter rises with increasing flow rate as there is a higher volume of polymer and greater mass transfer at the orifice. For example at 500 μL min^{-1}, the mean fiber diameter is 117 nm whereas at 2000 μL min^{-1}, the mean fiber diameter is 170 nm. When solvent evaporation and mass transfer are in equilibrium, low diameter fibers can be achieved. The shape and volume of the emerging polymer droplets can be altered by varying flow rates, having a marked effect on fiber size and distribution. At higher infusion rates, the production rate is generally greater due to the increased volume of material in the rotating vessel.

2.4. Pressure-Coupled Infusion Gyration

Fiber formation using pressure-coupled infusion gyration (PCIG) is governed by centrifugal force, dynamic fluid flow, and applied gas pressure.[46] In this system, the rotating aluminium vessel is connected to the gas inlet through an acrylic T-junction, while polymer solution is infused by a syringe pump. Variation of infusion rate allows for manipulation of the fiber diameter. Stretching of the polymer jet is enhanced at higher rotational speeds and centrifugal force. Solution blowing as a result of gas pressure causes further acceleration and manipulation of the polymer jet. PCIG allows for additional processing parameters to be considered for further tailoring of the final product morphology. It also allows polymers that are otherwise poorly spinnable to be processed into fibrous products.[47] For optimization of the system parameters, modeling of PCIG using response surface methodology is in progress. First results have shown that polymer concentration in solution and gas pressure may have a more significant effect on fiber morphology than previously known.[48]

2.5. Pressurized Melt Gyration

Pressurized melt gyration is a process of forming fibers that does not require the use of solvents. The absence of solvents unwraps potential in a variety of applications where cytotoxicity is a concern.[49] As with conventional gyration, pressurized melt gyration utilizes the identical apparatus setup but also incorporates a heating gun.[50] The temperature of the pot can be directly regulated and controlled by the heat gun, which is capable of producing temperatures of up to 400 °C. The high temperatures experienced in the gyration vessel induce a polymer melt, which undergoes the same forces at the vessel orifices as a polymer solution would.

Increased pot temperature reduces fiber diameter. At higher temperatures, the molten polymer remains in a liquid state for a longer duration, permitting a greater extent of jet stretching. As the molten polymer jet escapes from the orifices, exposure to the open environment causes rapid cooling and fibers are formed as a result of jet cooling and thinning. Furthermore, the viscosity of the melt reduces with increasing temperatures, which also attributes to the reduction in fiber diameter.[51] Low viscosity instigates additional stretching of the emerging jet and leads to the production of thinner fibers.

3. Properties of Materials

3.1. Solution Spinnability of Polymers

To date, many different polymers have been successfully spun into fibers using PG and it has been found that a variety of solvents can be combined to dissolve the same polymer. Diameters as low as 60 nm have been achieved. Unlike electrospinning and other fiber production methods, PG alleviates the need for an applied voltage, so the electrical properties of the spinning solution need not be considered.[52] Note that loading the solution into the vessel is slow and solvent evaporation can be an issue. As previously described, this can be avoided if an infusion method is used and the environment is controlled. **Table 1** shows the polymers that have been spun along with their concentration, molecular weight, and the solvent used. The potential applications of the fibers produced are given.

3.2. Mapping Solubility and Spinnability

Solvents must be carefully selected to ensure fibers can be produced in polymer–solvent systems. Solution parameters such as viscosity and molecular weight significantly affect the fiber outcome, so the appropriate criterion to produce fibers for a particular polymer must be confirmed. Moreover, the solvent will determine the critical minimum polymer concentration and chain entanglement, which must be optimized to yield fibers (rather than other morphologies, i.e., beads).

The spinnability of polyethylene terephthalate (PET) has been investigated. To determine whether a solvent with a high solubility for PET would yield fibers, a wide variety of solvents and solvent systems with varying solubility parameters were mapped onto a Teas graph. The solubility–spinnability region in various solvent systems was determined based on the time taken for it to dissolve in each system to form a homogenous solution.[33] By combining solubility and spinnability, a solvent with high solubility for PET (trifluoracetic acid) was found to produce nanofibers (**Figure 4**). Solvents with low solubility (formic acid and dichloromethane) were found to produce beads from the same concentration of solution (20 wt%).

A Teas graph was also used to help select a binary solvent system. A solvent with high solubility for PET, trifluoroacetic acid (TFA), and a non-solvent were used. Assuming that the combined solvents would have the same solubility parameters as those solvents with high solubility for PET, the solvent ratios were determined. For TFA + dichloromethane (DCM) a ratio of 1:1 was observed. For TFA + DMF and TFA + chloroform ($CHCl_3$) the ratio was 4:1. The parameters for the solvent TFA and DCM (1:1) were very close to those of TFA, which is known to dissolve PET and therefore the binary solvent system was expected to produce fibers.

Scaling laws were determined for the relationship between polymer concentration and viscosity using the solvents deemed appropriate from the Teas graph. Plots of specific viscosity against PET concentration revealed that increasing the weight percentage increased the specific viscosities. The scaling values were found to be in good agreement for the theoretical predictions for entangled solutions in a good solvent. The results demonstrated that there needs to be a minimum polymer concentration C_e for nanofiber generation, and therefore there must also be a minimum level of chain entanglement. Below C_e only beads are observed but, it should be noted, that the minimum polymer concentration will be different for different polymers, molecular weights, and solvent systems. PG allows for tailoring of the microstructural evolution so that beaded products can be generated.[38]

Following this, a mathematical model using rotational and blowing frames was developed and adapted from Mellado et al.[45] to elucidate a relationship between fiber diameter and experimental parameters such as fiber velocity, air velocity, kinematic viscosity, angular velocity of the vessel and the collector to vessel radius. r_1 is the initial jet radius, r_2 is the final jet radius, $\nu = \frac{u}{p}$ is the kinematic viscosity, R_c is the radius of the collector, U is the initial velocity and Ω is the angular velocity. V_a is the air velocity [Equation (1)].

$$r_2 = \frac{r_1 U^{3/2} \nu^{1/2}}{R_c^{3/2} \Omega V_a} \tag{1}$$

The final fiber radius results from competing surface tension, viscosity, rotation speed, and air velocity. In this first model for the PG process, only rotation speed, viscosity, and air velocity were varied to determine the effect on fiber diameter. This work shows the importance of mapping solvent–spinnability for a particular polymer solvent system. Using a Teas graph, polymer fibers can be designed through their solvent interactions prior to spinning using PG but ultimately, a greater understanding of the physical properties of the polymer solutions is needed to refine Equation (1), to predict r_2 and thus the final fiber diameter.

3.3. Properties of Fibers

Much like electrospinning, the ultimate processing goal is to maintain consistent fiber diameters at long lengths with controllable surface morphology. When these conditions are achieved PG will be scaled-up for manufacturing. **Table 2** reports the effect of varying PG parameters and their contribution to the aforementioned requirements. Currently PG is able to achieve such targets only with respect to certain polymers, for example poly(ethylene oxide) and polycaprolactone. Thus, more modeling-based research is necessary to elucidate the effect of these parameters on the outcome of different polymers.

4. Applications

4.1. Drug Delivery

In recent years, micro- and nanoscaled fibers have been increasingly used as drug-delivery vehicles.[64–66] Poor solubility of countless drugs can be overcome by dispersing the drug molecules within polymer solutions, which are then spun as fibers. PG and its sister processes provide an attractive manufacturing route for low diameter fibers, which have shown great potential

Table 1. Polymers spun in solution using pressurized gyration with or without modification.

Polymer	Solvent	Details (molecular weight or details of each polymer in copolymer/composite/blend)	Concentrations spun	Product characteristics [unless otherwise stated, fiber diameter in nm]	Application	Reference
Polyethylene oxide (PEO)	Distilled water	M_w 200 000 g mol^{-1}	5, 15, 21 wt%	60–1000	Aligned polymeric nanofibers	[30]
PEO, polyacrylic acid (PAA), sodium carboxymethylcellulose (CMC), sodium alginate	Distilled water	M_w CMC = approx. 250 000 g mol^{-1} M_w PEO = approx. 200 000 g mol^{-1} M_w PAA = 450 000 g mol^{-1} Sodium alginate = medium viscosity	15 wt% PEO/PAA 4.5 wt% 5 wt% PEO/CMC 4.5 wt% 15 wt% PEO/alginate 4.5 wt%	161–280	Vaginal drug delivery	[53]
Potato starch ($(C_6H_{10}O_5)_n$, amylose:amylopectin 25:75): PEO	Distilled water, dimethyl sulfoxide (DMSO) (50:50)	M_w PEO = 200 000 g mol^{-1} M_w starch = approx. 10^6 g mol^{-1}	PEO:Starch: 13.5:1.5 wt% (90:10) 11.5:4.5 wt% (70:30) 7.5:7.5 wt% (50:50)	160–650	Scaffolds for tissue engineering, protein drug release	[20]
PEO and DsRed-AuBP2-engineered protein	Distilled water	Infusion Gyration: M_w PEO: 200 000 g mol^{-1} DsRed-AuBP2-engineered protein: 30 kDa	5, 10, 15, 21 wt%	117–216	Biohybrid materials for imaging, sensing, and biomaterials	[44]
Poly-*N*-vinylpyrrolidone (PVP): Kollidon 25 (K25), Kollidon 30 (K30), and Kollidon 90F binder (K90F)	Phosphate-buffered saline (PBS) solution prepared using distilled water	M_w K25 = 28 000–34 000 g mol^{-1} M_w K30 = 44 000–54 000 g mol^{-1} M_w K90F = 1 000 000–1 500 000 g mol^{-1}	10, 20, 30% w/v (repeated for each binder)	462–971	Nanofiber meshes	[39]
Ibuprofen 25 (BCS II) (IBU) in PVP (Kollidon 90F)	Ethanol	M_w IBU = 206.28 g mol^{-1} M_w K90F = 100 000–150 000 g mol^{-1}	K90F concentration was fixed at 10% w/v, IBU concentration was adjusted to 10, 30, and 50%: IBU-K90F 10%, IBU-K90F 30% IBU-K90F 50%	1500–1900	Drug-loaded nanofibers for oral administration	[54]
Polyethylene (terephthalate) (PET)	Trifluoroacetic acid, trichloroacetic acid, dichloromethane, chloroform, dimethyformaldehyde (all in various mixtures)	M_w PET = 100 000 g mol^{-1}	5, 10, 15, 20, 25 wt%	290–675	Potential use in filters	[33]
Nylon 6,6 modified with functional Ag nanoparticles (NPs).	Formic acid (aqueous Ag NPs)	M_w nylon 6,6 = 30 000 g mol^{-1} Particle size Ag NPs = 150 nm	Nylon + Ag: 5 + 0 wt% 10 + 0 wt% 15 + 0 wt% 20 + 0 wt% 5 + 1 wt% 10 + 1 wt% 15 + 1 wt% 20 + 1 wt%	Nylon: 59–470 Nylon + Ag: 57–152	Antibacterial fiber mats	[55]
Poly(vinyl alcohol) (PVA), lysozyme from chicken egg white, Au NPs	PBS, distilled water	M_w PVA = 146–186 kDa, 87–89% hydrolyzed M_w lysozyme = 14.3 kDa, ≈70 000 U mg^{-1} Average diameter Au NPs ≈10 nm	Au nanoparticle solution and PVA-lysozyme solution with v/v ratios of 1:10, 1:5, and 2:5 were used to prepare gold-nanoparticle-encapsulated microbubbles.	Bubble diameter = 50–450 µm	Antibacterial microbubbles with biosensing capabilities	[56]
PCL, Silver (Ag) NPs	Triethylene glycol monomethyl ether for Ag NP suspension	Pressurized melt gyration: Mn PCL ≈ 80 000 Particle size Ag NPs = 10–150 nm	PCL-95 °C, PCL-105 °C, PCL-125 °C, PCL-150 °C, PCL-155 °C, PCL-200 °C PCL-Ag 95 °C, PCL-Ag 125 °C, PCL-Ag 155 °C, PCL-Ag 200 °C Ag NP solution: 0.01% v/v	14–38 µm	Antibacterial mats, wound healing	[50]

Table 1. (Continued).

Polymer	Solvent	Details (molecular weight or details of each polymer in copolymer/composite/blend)	Concentrations spun	Product characteristics [unless otherwise stated, fiber diameter in nm]	Application	Reference
Graphene–SiOC/PVP n	Chloroform and dimethylformamide (DMF) binary solvent	(B1) Polymethyl-silsesquioxane (MK) resin solution (M_w = 9100 g mol^{-1}) (B2) Polymethylphenyl-silsesquioxane (H44) resin solution (M_w = 2100 g mol^{-1}) (B3) H44 + 3% graphene solution M_w PVP ≈1 300 000 Da (Sn containing dibutyltindilaurate and Zr-acetylacetonate were used as catalysts for MK and H44 resins, respectively)	(B1) MK/PVP: 25 wt% resin (B2) H44/PVP: 20.7 wt% resin (B3) H44/ PVP/graphene: 20.7 wt% resin	1000–5000	Industrial ceramics	[57]
Polyacrylonitrile (PAN), polymethylmethacrylate (PMMA)	DMF	M_w PAN = 150 000 g mol^{-1} M_w PMMA = 120 000 g mol^{-1}	S1 PAN: 4% w/v S2 PAN: 8% w/v S3 PAN:10% w/v S4 PMMA: 30% w/v S5 50:50 PAN–PMMA (20% w/v total polymer)	290–580	Porous nanofibers	[58]
PCL	Acetone	M_w PCL = 80 000	5, 10, 15, 20, 25, and 30 wt%	≈351 µm	Beads on a string for drug carrying	[38]
Graphene nanoplatelets (GNPs) loaded thermoplastic polyurethane (TPU) and phenolic resin (PR)	DMF	TPU, Desmopan DP 9855DU PR, (Bayer, Italy) GNPs ≈ 964 × 457 nm (L × W) M_w PVP ≈1 300 000 Da	15% TPU-5%GNP 20% TPU-5%GNP 25% TPU-5%GNP 10% PR-10%PVP 15% PR-10%PVP 20% PR-10%PVP 10% PR-10%PVP-5%GNP 15% PR-10%PVP-5%GNP 20% PR-10%PVP-5%GNP 0.75	1000–9000	Graphene reinforced composites	[59]
PAN-based graphene nanoplatelet loaded fibers	DMF	M_w PAN = 150 000 g mol^{-1} GNPs: ≈2 nm, diameter of 1–2 µm, average surface area of ≈750 m^{2}g^{-1}, and bulk density of ≈0.2 g cm^{-3}	GNPs (0, 0.2, 1.0, 3.0, and 8.0 wt%) dispersed in PAN solution (10 wt% PAN in DMF)	1000–5000	Carbon nanofibers	[60]
PAN, cellulose acetate (CA), and (PAN-CA)	DMF, acetone	M_w PAN = 150 kDa M_w CA = 30 kDa	PAN solutions (5, 10, 15 wt%) CA solutions (15, 20, 25 wt%) 10 wt% PAN-CA	200–2000	Porous structures for electrochemistry	[61]
Antimicrobial nanoparticle (AMNP) loaded PMMA fibers	Chloroform	M_w PMMA = 120 000 g mol^{-1} Antimicrobial nanoparticles (two types: AMNP1 and AMNP2) (University of Hertfordshire)	K0 20% w/w PMMA K1 0.1% AMNP1 loaded w/w PMMA K2 0.25% AMNP1 loaded w/w PMMA K3 0.5% AMNP1 loaded w/w PMMA K4 0.1% AMNP2 loaded w/w PMMA K5 0.25% AMNP2 loaded w/w PMMA K6 0.5% AMNP2 loaded w/w PMMA	6–20 µm	Antimicrobial filters	[62]
Poly(*L*-lactide)/poly(methyl methacrylate) (PLLA)/PMMA + hydroxyapatite (HA) nanopowder	Chloroform	PLLA (amine-terminated, average Mn 2500, polydispersity ≤ 1.3), PMMA (average Mn 1 20 000) HA particle size ≤ 200 nm	PLLA/PMMA 50:50, 20 wt%	≈17 µm	Mechanically active bone tissue scaffolds	[63]
PEO	Water	Pressure-Coupled Infusion Gyration PEO, M_w 200 000	(3, 5, 10, 15, and 21 wt%)	100–2400	Oriented polymeric fiber mats	[46]

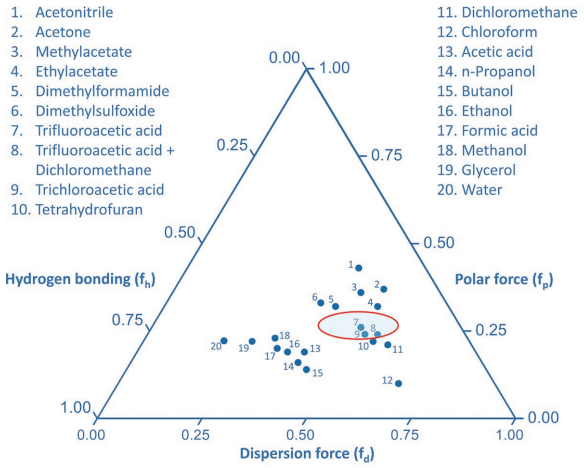

Figure 4. Teas graph showing solubility–spinnability map of PET. Circled region shows the selection of a binary solvent system. Adapted with permission under the terms of the CC BY 4.0 license.[33] Copyright 2015, The Authors. Published by Elsevier B.V.

in drug delivery. In fact, recently prepared polymer-magnetic composite fibers fabricated by infusion gyration have been successful in remote-controlled drug release.[67]

Drugs in crystalline form possess strong intermolecular bonds that require a higher energy barrier to dissolution, leading to lower solubility.[68] By solubilizing a drug with a suitable solvent, it is converted into its amorphous form and the energy barrier to dissolution is lowered.[69] The amorphous solution can then be mixed with a hydrophilic polymer solution and processed into fibers using PG. The resulting fibers hold the amorphous drug molecules via steric hindrance of the polymer chains. As the hydrophilic polymer dissolves, drug molecules are released as fine colloidal particles.[70] The high surface area to volume ratio of these fibers further enhances drug dissolution due to the increased contact area to the dissolution media.[71] PG overcomes a significant limitation in the large-scale manufacture of micro- and nanofibrous drug systems, allowing for production rates in excess of kilograms per hour.[39]

Table 2. Effect of pressurized gyration parameters on fiber diameter and/or fiber surface.

Parameter		Fiber properties
Process parameters	↑ Working pressure	↓ Fiber diameter
	↑ Rotational speed	↓ Fiber diameter
Solution parameters	↑ Polymer molecular weight	↑ Fiber diameter
	↑ Polymer concentration (viscosity)	↑ Fiber diameter
	↑ Solvent volatility	↓ Fiber diameter
		↑ Pore size on fiber surface as evaporation increases
System parameters	↑ Orifice size	↑ Fiber diameter
Ambient	↑ Temperature	No effect unless temperature is increased much higher as with pressurized melt gyration
	↑ Relative Humidity	↓ Uniformity

↑ and ↓ denote increase and decrease respectively. It should be noted that these are the most common overall outcomes and exceptions may exist for some polymer systems and polymer concentrations used.

PG was used to prepare fibers with varying percentage loadings of ibuprofen dispersed in polyvinylpyrrolidone (PVP).[54] Dispersions of ibuprofen demonstrated a significant increase in drug-release rate when compared to the drug powder. As drug content increased, solution viscosity, and surface tension increased. Such qualities have a marked effect on bead size, fiber diameter, and even jet stability, yet drug-loaded fibers did not differ in surface topography compared to unloaded fibers.[20,72–74] Drug content increased as fiber diameter increased, concurrent with literature values.[66,75] X-ray diffraction patterns confirmed the presence of amorphous drug within the fibers, explaining increased solubility. Fourier transform infrared spectroscopy (FTIR) data evidenced strong drug–polymer hydrogen bonding. Rapid solvent evaporation during the PG process allowed for the production of fibers with complete drug–polymer miscibility. This was confirmed by modulated temperature differential scanning calorimetry (DSC), where a single glass transition temperature (T_g) was detected.

PG has been used to prepare nanofibers with mucoadhesive properties for use in vaginal therapy.[53] Drug delivery to the mucosal sites of the body is advantageous as it improves patient compliance and topical targeting. Nanofibers are valuable in topical and mucosal drug delivery due to their high surface area to volume ratio, enabling delivery across the mucosal barriers—where highly bulky and hydrophilic peptide and protein drugs would otherwise have difficulty.[76] Two highly mucoadhesive polymers, carboxymethyl cellulose and polyacrylic acid, were prepared as blends using PEO as a carrier, yielding well-defined and uniformly cylindrical fibers with high structural integrity. FTIR data established the presence of mucoadhesive properties. Atomic force microscopy was used to further confirm mucoadhesive properties of the fibers with simulated vaginal mucin, demonstrating significant potential of the fibers for use in vaginal therapy.[77]

In a separate but related study, PG was used to develop progesterone-loaded bioadhesive nanofibers as a drug-delivery system for reduced incidence of preterm birth.[78] Polyethylene oxide and carboxymethyl cellulose were chosen as carrier polymers due to their mucoadhesive properties. Hot-stage microscopy was used to confirm the presence of progesterone within the polymeric fibers. Depending on the polymer compositions, the resulting fiber diameters ranged from 40 to 1000 nm. A high (25 wt%) loading of progesterone was achieved. The nanofibers indicated a higher and more uniform drug-release when compared to a commercially available progesterone pessary (Cyclogest). Nanofibers produced using PG have enabled the delivery of progesterone to the vaginal mucosal membrane where incorporation of poorly water-soluble drugs into hydrophilic nanofiber carriers is particularly challenging.

Fibers produced by PG demonstrated more rapid drug release compared to those produced using electrospinning. Amphotericin B and itraconazole, two poorly water-soluble drugs, were dispersed within polymeric fibers produced using both electrospinning and PG. The morphology of the fibers constructed by

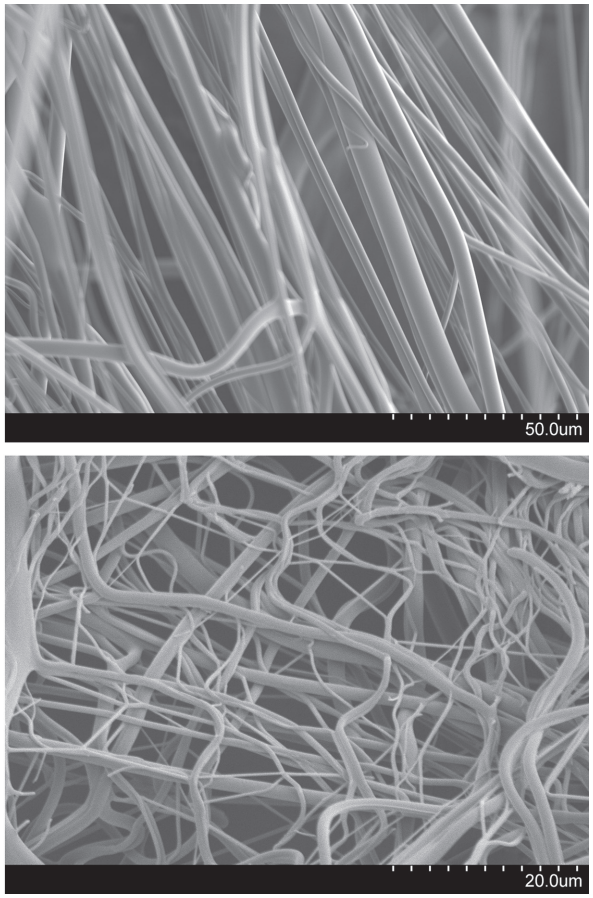

Figure 5. Scanning electron microscopy images of a) pressurized gyration drug-loaded fibers possessing a uniaxially aligned profile and b) electrospun drug-loaded fibers showing an overlapping profile.

the two techniques differed **(Figure 5)**, which may explain the differences in their drug release profiles.[79] Previously, incorporation of uniformly dispersed drugs into electrospun fibers was hindered by the low yield of the method.[9] PG allows for significant fiber production rates in a single step and has the potential to be scaled further.

4.2. Tissue Engineering

Polymer nanofibers have shown significant promise in tissue engineering applications.[80] The high surface area to volume ratio provides ideal conditions for the formation of an extracellular matrix (ECM) to match that of native tissue.[81] Not only this, the aligned fibers offer directionality to cell growth and can enhance the deposition of cells and the attraction of ECM factors such as collagen and elastin.[82] Conventional PG relies on the use of solvents which is a potential drawback in the creation of tissue engineered constructs. Melt-spinning with regulated temperatures allows for good control over surface roughness, an essential property that influences cellular infiltration.

In the first study of its kind, a pressurized melt gyration process was developed to evade the use of cytotoxic solvents in polymer solutions. A heat gun was used in conjunction with PG apparatus and applied to the rotating vessel to produce nonwoven PCL and Ag-loaded PCL-based fiber scaffolds with antibacterial properties.[50] Xu et al. obtained PCL scaffolds at melt temperatures of 95, 125, 155, and 200 °C at varying working pressures and rotating speeds. To evaluate the antibacterial activity, Ag-loaded PCL fibers were produced using Ag coated pellets that were melt-spun at different temperatures using gyration at a speed of 36 000 rpm and 0.01 w/v NP solution.[50]

Fiber diameter was found to be related to melt temperature. As the temperature increased, fiber diameter reduced. For the PCL molten polymer, increasing the temperature from 95 to 200 °C reduced the fiber diameter from 38 to 28 µm. Increased rotational speed further decreased the fiber diameter to 18 µm. As the temperature was increased from 105 to 200 °C and the working pressure was increased from 0.1 to 0.2 MPa, the fiber diameter was reduced to 15 µm. The effects of working pressure and speed are therefore consistent with what is expected for PG. When temperature is increased, the molten liquid jet remains in a liquid state for longer, causing additional stretching of the polymer fiber jet. Rapid cooling occurs at the orifice. The polymer melt viscosity is also reduced at higher temperatures, so thinner fibers are achieved with increased stretching time and lowered melt viscosity.

The melt temperature of PCL was also found to directly influence the surface morphology of the scaffolds. Xu et al. found that above 105 °C, surface roughness was observed and at 155 and 200 °C, extrusion lines were visible on the surface of the fibers, as well as fibril lines and pits.[50] Raman spectra of the PCL scaffolds were used to confirm an increase in crystallinity associated with increase in temperature. For the Ag-coated PCL scaffolds, no significant difference in molecular structure was observed following Raman spectroscopy, although microanalysis in the wavelength 1700–1760 cm^{-1} showed differences in crystallinity, indicating that nanoparticle incorporation prevents the movement of molecular chains and thus decreases the crystallinity.

Antibacterial activity was significantly higher for the Ag-coated PCL scaffolds than the PCL control when evaluated using both *Escherichia coli* and *Pseudomonas aeruginosa*. Melt-spun scaffolds also proved to be biocompatible with no signs of toxicity to the C2C12 cell line and percentage cell proliferation was found to be highest at 95 °C. DAPI (4',6-diamidino-2-phenylindole) staining was used to confirm that there was a high amount of cell attachment and cell spreading at this temperature compared to others. Cellular infiltration was found to be highest at 155 °C, where the scaffold porosity was large enough to allow cells to move inside the scaffolds. This research shows the potential of pressurized melt gyration in the production of biocompatible fiber mats and the possibilities of using melt temperature to control the morphology and topography of fibers.

4.3. Diagnostics

The application of nanofibers to the development of biosensors and medical diagnostic devices has seen intense interest.[83–85] Biosensors encompass a wide range of devices that are used in the detection of various analytes. The versatility of nanofibers

in terms of high surface area, porosity, surface architecture, and topography provide great practicality and potential as biosensing membranes.[86]

PG allows for the generation of particles and bubbles in addition to fibers. Microbubbles can be achieved at a higher production rate than those produced using microfluidics or sonication. Bubbles are formed as the polymer solution-filled vessel rotates. With simultaneous application of gas pressure and pot rotation, the external forces combine to create an intense vortex leading to deformation of the polymer surface. As the rotational speed increases, air penetrates through the core of the emerging jet, causing it to shrink and move from a stable to an unstable state, producing microbubbles.[35] Rapid central rotation of the vessel funnels the flow around the apex of the vortex and is followed by a pinching-off process, leading to bubble formation.

Protein-coated microbubbles can be made using PG to enhance their stability for use in a wide range of biomedical applications—ranging from medical imaging to drug delivery.[87–89] A reduction in average microbubble diameter is generally observed with increasing rotational speeds above the critical minimum speed. The nanoparticle content of the solution can also affect the diameter and size distribution of the bubbles produced. A dramatic reduction in microbubble diameter is observed with increasing applied gas pressure. Although PG offers a high-volume production route, monodisperse microbubble production for use in biomedical engineering has not yet been achieved and more research is needed in this area.

4.4. Hydrogels

Swelling to hold vast amounts of water, hydrogels are cross-linked hydrophilic polymer networks that are resistant to dissolution.[90] Their responsiveness to a number of environmental stimulants makes them effective in various biomedical settings.[91,92] Cross-linking allows for superior control over physical properties such as viscosity and solubility, forming 3D insoluble networks from which bioactive molecules can be released.[93] Physical cross-linking allows for the formation of reversible hydrogels, although this can lead to network defects. Permanent or chemical cross-linking, can be achieved through covalent bonding.

Common methods for chemical cross-linking often result in weak and brittle hydrogels, which are therefore limited in their application.[94] As crosslinking is unable to occur at regularly separated positions, there is a broad distribution in the length of the chains between cross-linking points. Not only this, the cross-linking density and inter-crosslinking molecular weight cannot be controlled separately. When the concentration of the cross-linker is high, heterogeneous aggregation of the cross-linking points occurs.[95] Hydrogels that have been chemically cross-linked are thus limited in terms of their morphology, mechanical strength, and optical transparency.[96] Although ultra-stretchable, self-healing, and tough hydrogels can be synthesized through physically cross-linking, for example, from polyacrylamide-montmorillonite (PAM-MMT), it is difficult to achieve low hysteresis, and therefore optimum mechanical properties, as some of the organic–inorganic cross-links will break. Much research is therefore focused on improving the properties of chemically cross-linked hydrogels.

Our laboratory, in association with Chen and coworkers, used PG to fabricate PAM-clay nanocomposite hydrogel fibers, exhibiting low hysteresis.[95] To do this, in situ polymerization of acrylamide (AM) in the presence of MMT or chitosan–treated MMT (CHI–MMT) was conducted at 60 °C, instead of with a catalyst, to allow for chain grafting and branching. The radical initiator attacked the hydroxyl groups of the polysaccharide chains to generate alkoxy radicals, initiating polymerization of AM. No chemical cross-linker was used and the mechanical properties of the nanocomposite hydrogels, prior to swelling and when fully swollen, were measured.

PAM-MMT and PAM/CHI–MMT (with chitosan) hydrogel fibers were fabricated from precursor materials: water, MMT, chitosan, initiator, and monomer. It was found that both hydrogels had high strain and that treating with chitosan improved physical properties due to electrostatic interactions. Furthermore, both hydrogels in this work demonstrated resilience due to strong interactions within the hydrogels as a result of chain branching, multiple hydrogen bonding, covalent bonding, and/or electrostatic force. The exceptional hysteresis results, high strength, and resilience of the nanocomposite hydrogels can be applied to fiber production using the PG method, having potential application in many biomaterials areas, due to their ease of processing.

4.5. Filtration

Owing to their high surface area to volume ratio and enhanced porosity, fibers produced using PG are excellent materials for filtration.[97] Application of fibers in filters can be divided into liquid and air filtration systems.[98] Polymeric sub-micron-sized fibers are used mostly in porous membranes for ultrafiltration (excluding particle sizes of 100 nm upward) or nanofiltration (excluding particle sizes that are just a few nanometers). Mostly these are carbon-based filters that can be used for removing contaminants from wastewater, such as phenols, or for the purification of drinking water and removal of pesticides.[99–101] Air filtration applications include dust collectors and protective clothing and importantly, antibacterial hospital filter systems, which are becoming increasingly used in the fight against antibacterial resistance.[102]

As infectious diseases and antibiotic resistance become increasingly prevalent, there is greater focus on ultrafiltration with the incorporation of nanoparticles.[103,104] To produce antimicrobial ultrafiltration systems for air, tellurium (Te) nanoparticles were embedded into a PMMA mesh using PG.[105] Porous PMMA fibers with 1, 2, and 4 wt% Te particles were prepared, and SEM was used to confirm dispersion of antimicrobial Te particles. Increased concentration of Te particles led to wider diameter fibers, from 0% loaded Te fibers having diameters of 7.06 ± 3.77 μm to 4% loaded Te fibers having diameters of 13.9 ± 7.05 μm. Pore size was found to decrease with increased fiber diameters and increased Te loading. Te/PMMA fiber meshes exhibited antibacterial activity toward Gram-negative *E. coli*, a common cause of hospital acquired infection. The bactericidal activity of Te/PMMA fibers was dose-dependent

and increased as the percentage loading of Te increased. These findings demonstrate the feasibility of Te as an alternative to silver nanoparticles, a well-established antibacterial agent.[106] In fact, PG is a powerful method by which novel antimicrobial agents can be incorporated in polymeric mesh-like filters and bandages.[107]

4.6. Wound Healing

PG offers an amenable approach to the mass production of fiber mats. Bacterial cellulose (BC), a notoriously difficult polymer to process, has been blended with PMMA, to produce BC:PMMA bandage-like scaffolds.[108] BC possesses exceptionally high water-holding ability, a fine microfibril network and enhanced cell compatibility, making it a highly suitable material for use in wound healing (**Figure 6**).[109,110] BC solutions alone cannot form fibers but PG has afforded the BC:PMMA solutions to yield fibers that had fiber diameters as low as 690 nm. PG was further capable of rapid bandage generation with exceptionally high yields. The mat produced resembled bandages that could be used directly, requiring no further modification.

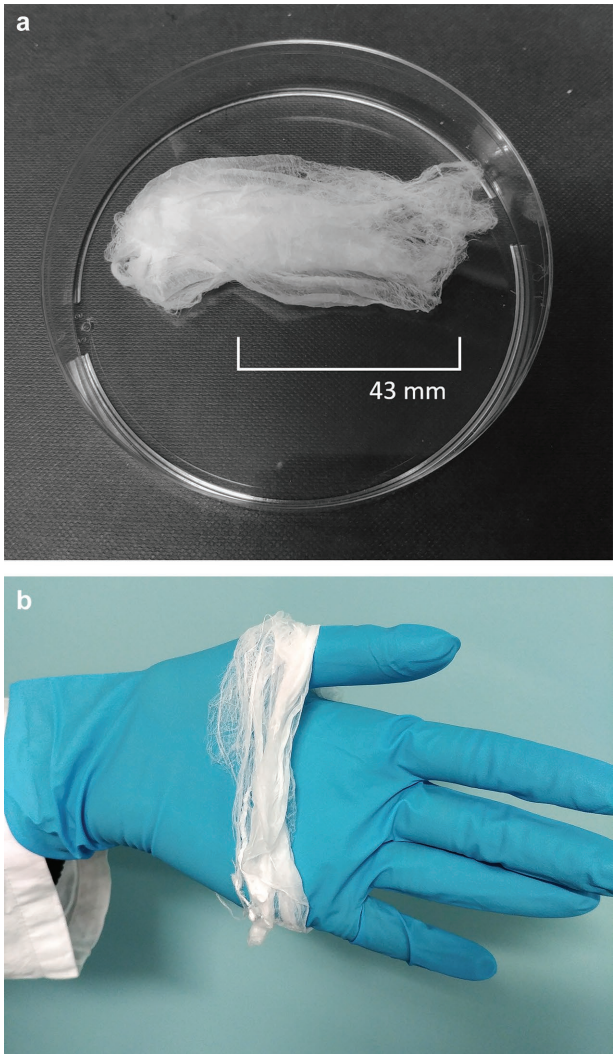

Figure 6. Polycaprolactone fibers produced via pressurized gyration, demonstrated as a) a patch and b) a wearable bandage.

5. Future Perspectives

Herein, an extensive number of applications for PG and its sister technologies have been showcased. The possibilities that this exciting fiber-processing method offer are by no means limited to these examples and due to the modular and facile nature of this system; we are confident that further modifications and uses for polymers produced with this technique will be revealed.

Unlike electrospinning, PG does not require the use of an electric field. So far, electrospinning has had limited scalability due to problems with charge interferences in multiple-needle setups.[111] The PG setup is capable of spinning 5 mL of polymer solution in under 15 s whereas, electrospinning will typically produce fibers at 50 µL min^{-1} due to limits set by low infusion rates.[112] Infusion gyration is capable of producing fibers at 5000 µL min^{-1}, providing a yield of 1.45 kg h^{-1}; furthermore, PG (Mark I) is capable of producing even higher fiber yields.[20,34] Therefore, PG allows for high production rates that are orders of magnitude higher than electrospinning. Production rate coupled with scalable design enables the setup to produce fibers on an industrially relevant scale, in excess of other commercially available fiber production technologies.[112] Even compared to commercially available electrospinning techniques the production rates are far greater.[26] There are no obstacles that prevent its scale-up and the design can be reconfigured by changing orifice density and shape, as well as the vessel volume to increase yield.

PG is able to spin a large number of polymers with or without the requirement of solvents. Melt gyration offers the possibility of producing fibers from a large range of polymers by avoiding non-economical and/or hazardous solvents. The in situ melting of the polymer within the gyration vessel allows for a scalable and simple approach to manufacturing small-diameter fibers. In the spinning of fibers for biomedical applications, the use of certain solvents can lead to the rejection of the final material by the Food and Drug Administration. Many of the commonly used solvents such as chloroform and dichloromethane are not desired in biomedical applications. Melt gyration forms fibers free from harsh solvents and thus eliminates further concern to health and safety.

Collection of the emerging fibers in the form of a drying polymer jet is crucial to the morphology of the final fiber product. By incorporating different collection techniques, fibers can be produced with varying morphologies. If highly aligned fibers are desired, then a collector that mimics the rotation of the vessel can be created to gather aligned fibers. Stationary and dynamic collectors permit the almost-limitless modification of fiber morphology to suit various biomedical applications.

The rotational speed of the gyration vessel can determine fiber diameter and length. By incorporating updated and modified designs, the rotational speed can be increased to result in the manufacture of thinner diameter fibers with a higher production rate. The internal volume of the rotating vessel can

be scaled accordingly to increase production rate and fiber continuity. Orifice count can be increased or decreased to control the fiber production rate. Control of orifice diameter and shape permits the highly customizable fabrication of fiber products with varying morphology and properties. A reduction in orifice diameter can furthermore lead to the formation of smaller diameter fibers. Computational 3D modeling can be incorporated to test the effects of varying vessel dimensions and materials on the production and scalability of micro- and below fibers. Solution properties, such as viscosity and polymer melt molecular weight, are also known to have a marked effect.

The creation of core–sheath polymer fibers generated using a novel PG process is in progress. The newly designed spinneret consists of inner and outer vessels which can accommodate two different polymer solutions to generate core–sheath structures. This design is also useful for the formation of novel structures and encapsulation of other constituents such as drugs, nanoparticles, and bioactive agents. In this core–sheath polymer fiber manufacturing research, we show that the new technology could be used to process different polymer solutions and to successfully encapsulate nanoparticles. Future iterations of this technology bring great promise in the advancement of fiber technologies and their applications.

Acknowledgements

P.L.H. and J.A. contributed equally to this work. This work was supported by the UK Engineering and Physical Sciences Research Council (grants EP/L023059/1, EP/N0342281). We are also grateful for many international and UK collaborations (e.g., USA, China, Turkey, Italy), which have introduced variation and extra innovation to the work. The authors wish to thank BASF for also supporting our gyration research, in particular James Hart, Manager of Technical Service Pharma Ingredients & Services Europe.

Conflict of Interest

The authors declare no conflict of interest.

Keywords

fibers, pressurized gyration, polymers, biomedical, functional

Received: April 10, 2018
Revised: May 22, 2018
Published online:

[1] S. Ramakrishna, K. Fujihara, W.-E. Teo, T. Yong, Z. Ma, R. Ramaseshan, *Mater. Today* **2006**, *9*, 40.
[2] M. Zhu, J. Han, F. Wang, W. Shao, R. Xiong, Q. Zhang, H. Pan, Y. Yang, K. Samal Sangram, F. Zhang, C. Huang, *Macromol. Mater. Eng.* **2016**, *302*, 1600353.
[3] C. M. Hsu, S. Shivkumar, *Macromol. Mater. Eng.* **2004**, *289*, 334.
[4] H. Cho, S. Y. Min, T. W. Lee, *Macromol. Mater. Eng.* **2013**, *298*, 475.
[5] K. P. De Jong, J. W. Geus, *Catalysis Reviews* **2000**, *42*, 481.
[6] W. J. Li, C. T. Laurencin, E. J. Caterson, R. S. Tuan, F. K. Ko, *J. Biomed. Mater. Res.* **2002**, *60*, 613.
[7] L. Viry, S. E. Moulton, T. Romeo, C. Suhr, D. Mawad, M. Cook, G. G. Wallace, *J. Mater. Chem.* **2012**, *22*, 11347.
[8] Q. P. Pham, U. Sharma, A. G. Mikos, *Tissue Eng.* **2006**, *12*, 1197.
[9] C. J. Luo, S. D. Stoyanov, E. Stride, E. Pelan, M. Edirisinghe, *Chem. Soc. Rev.* **2012**, *41*, 4708.
[10] P. X. Ma, R. Zhang, *J. Biomed. Mater. Res.* **1999**, *46*, 60.
[11] H. Lu, L. Zhang, W. Xing, H. Wang, N. Xu, *Mater. Chem. Phys.* **2005**, *94*, 322.
[12] H. G. Chae, Y. H. Choi, M. L. Minus, S. Kumar, *Compos. Sci. Technol.* **2009**, *69*, 406.
[13] G. Whitesides, J. Mathias, C. Seto, *Science* **1991**, *254*, 1312.
[14] X. Zhang, Y. Lu, *Polym. Rev.* **2014**, *54*, 677.
[15] C. J. Ellison, A. Phatak, D. W. Giles, C. W. Macosko, F. S. Bates, *Polymer* **2007**, *48*, 3306.
[16] J. Shao, C. Chen, Y. Wang, X. Chen, C. Du, *React. Funct. Polym.* **2012**, *72*, 765.
[17] G. Chang, J. Shen, *Macromol. Mater. Eng.* **2011**, *296*, 1071.
[18] J. A. Ajao, A. A. Abiona, S. Chigome, A. Y. Fasasi, G. A. Osinkolu, M. Maaza, *J. Mater. Sci.* **2010**, *45*, 2324.
[19] H. Hou,C. Cheng, S. Chen, X. Zhou, L. Xiaoyi, P. He, X. Kuang, J. Ren, *US Patent 20130164629*, **2015**.
[20] S. Mahalingam, G. G. Ren, M. Edirisinghe, *Carbohydr. Polym.* **2014**, *114*, 279.
[21] N. Obregon, V. Agubra, M. Pokhrel, H. Campos, D. Flores, D. De la Garza, Y. Mao, J. Macossay, M. Alcoutlabi, *Fibers* **2016**, *4*, 20.
[22] R. T. Weitz, L. Harnau, S. Rauschenbach, M. Burghard, K. Kern, *Nano Lett.* **2008**, *8*, 1187.
[23] A. M. Loordhuswamy, V. R. Krishnaswamy, P. S. Korrapati, S. Thinakaran, G. D. Rengaswami, *Mater. Sci. Eng.: C.* **2014**, *42*, 799.
[24] V. Agubra, L. Zuniga, D. De la Garza, L. Gallegos, M. Pokhrel, M. Alcoutlabi, *Mater. Today* **2016**, *286*, 72.
[25] K. Sarkar, C. Gomez, S. Zambrano, M. Ramirez, E. de Hoyos, H. Vasquez, K. Lozano, *Mater. Today* **2010**, *13*, 12.
[26] J. J. Rogalski, C. W. M. Bastiaansen, T. Peijs, *Nanocomposites* **2017**, *3*, 97.
[27] K. Smoukov Stoyan, T. Tian, N. Vitchuli, S. Gangwal, P. Geisen, M. Wright, E. Shim, M. Marquez, J. Fowler, D. Velev Orlin, *Adv. Mater.* **2015**, *27*, 2642.
[28] A. Tokarev, O. Trotsenko, M. Griffiths Ian, A. Stone Howard, S. Minko, *Adv. Mater.* **2015**, *27*, 3560.
[29] A. Tokarev, D. Asheghali, M. Griffiths Ian, O. Trotsenko, A. Gruzd, X. Lin, A. Stone Howard, S. Minko, *Adv. Mater.* **2015**, *27*, 6526.
[30] S. Mahalingam, M. Edirisinghe, *Macromol. Rapid Commun.* **2013**, *34*, 1134.
[31] Y. Lu, Y. Li, S. Zhang, G. Xu, K. Fu, H. Lee, X. Zhang, *Eur. Polym. J.* **2013**, *49*, 3834.
[32] J. L. Daristotle, A. M. Behrens, A. D. Sandler, P. Kofinas, *ACS Appl. Mater. Interfaces* **2016**, *8*, 34951.
[33] S. Mahalingam, B. T. Raimi-Abraham, D. Q. M. Craig, M. Edirisinghe, *Chem. Eng. J.* **2015**, *280*, 344.
[34] X. Xu, J. Luo, *Appl. Phys. Lett.* **2007**, *91*, 124102.
[35] S. Mahalingam, B. T. Raimi-Abraham, D. Q. M. Craig, M. Edirisinghe, *Langmuir* **2015**, *31*, 659.
[36] K. Arayanarakul, N. Choktaweesap, D. Aht-ong, C. Meechaisue, P. Supaphol, *Macromol. Mater. Eng.* **2006**, *291*, 581.
[37] J. M. Deitzel, J. Kleinmeyer, D. Harris, N. C. B. Tan, *Polymer* **2001**, *42*, 261.
[38] X. Hong, M. Edirisinghe, S. Mahalingam, *Mater. Sci. Eng.: C* **2016**, *69*, 1373.
[39] B. T. Raimi-Abraham, S. Mahalingam, M. Edirisinghe, D. Q. M. Craig, *Mater. Sci. Eng.: C* **2014**, *39*, 168.
[40] E. U. Illangakoon, S. Mahalingam, K. R. Matharu, M. Edirisinghe, *Polymers* **2017**, *9*.
[41] Z. Wang, C. Zhao, Z. Pan, *J. Colloid Interface Sci.* **2015**, *441*, 121.

[42] N. Zhan, Y. Li, C. Zhang, Y. Song, H. Wang, L. Sun, Q. Yang, X. Hong, *J. Colloid Interface Sci.* **2010**, *345*, 491.
[43] G. Eda, S. Shivkumar, *J. Appl. Polym. Sci.* **2007**, *106*, 475.
[44] S. Zhang, B. T. Karaca, S. K. VanOosten, E. Yuca, S. Mahalingam, M. Edirisinghe, C. Tamerler, *Macromol. Rapid Commun.* **2015**, *36*, 1322.
[45] P. Mellado, H. A. McIlwee, M. R. Badrossamay, J. A. Goss, L. Mahadevan, K. Kit Parker, *Appl. Phys. Lett.* **2011**, *99*, 203107.
[46] X. Hong, S. Mahalingam, M. Edirisinghe, *Macromol. Mater. Eng.* **2017**, *302*, 1600564.
[47] M. Parhizkar, S. Mahalingam, S. Homer-Vanniasinkam, M. Edirisinghe, *Nanomedicine* **2017**, *13*, 5.
[48] X. Hong, A. Harker, M. Edirisinghe, *ACS Omega* **2018**, *3*, 5470.
[49] T. D. Brown, F. Edin, N. Detta, A. D. Skelton, D. W. Hutmacher, P. D. Dalton, *Mater. Sci. Eng. C Mater. Biol. Appl.* **2014**, *45*, 698.
[50] Z. Xu, S. Mahalingam, P. Basnett, B. Raimi-Abraham, I. Roy, D. Craig, M. Edirisinghe, *Macromol. Mater. Eng.* **2016**, *301*, 922.
[51] J. Vera-Sorroche, A. L. Kelly, E. C. Brown, T. Gough, C. Abeykoon, P. D. Coates, J. Deng, K. Li, E. Harkin-Jones, M. Price, *Chem. Eng. Res. Des.* **2014**, *92*, 2404.
[52] C. J. Luo, E. Stride, M. Edirisinghe, *Macromolecules* **2012**, *45*, 4669.
[53] F. Brako, B. Raimi-Abraham, S. Mahalingam, D. Q. M. Craig, M. Edirisinghe, *Eur. Polym. J.* **2015**, *70*, 186.
[54] B. T. Raimi-Abraham, S. Mahalingam, P. J. Davies, M. Edirisinghe, D. Q. Craig, *Mol Pharm* **2015**, *12*, 3851.
[55] Z. Xu, S. Mahalingam, J. L. Rohn, G. Ren, M. Edirisinghe, *Mater. Sci. Eng. C* **2015**, *56*, 195.
[56] S. Mahalingam, Z. Xu, M. Edirisinghe, *Langmuir* **2015**, *31*, 9771.
[57] S. Mahalingam, G. Pierin, P. Colombo, M. Edirisinghe, *Ceram. Int.* **2015**, *41*, 6067.
[58] U. E. Illangakoon, S. Mahalingam, P. Colombo, M. Edirisinghe, *Surf. Innovations* **2016**, *4*, 167.
[59] A. Amir, S. Mahalingam, X. Wu, H. Porwal, P. Colombo, M. J. Reece, M. Edirisinghe, *Compos. Sci. Technol.* **2016**, *129*, 173.
[60] X. Wu, S. Mahalingam, A. Amir, H. Porwal, M. J. Reece, V. Naglieri, P. Colombo, M. Edirisinghe, *ACS Omega* **2016**, *1*, 202.
[61] S. Mahalingam, X. Wu, M. Edirisinghe, *Mater. Des.* **2017**, *134*, 259.
[62] U. E. Illangakoon, S. Mahalingam, K. Wang, Y. K. Cheong, E. Canales, G. G. Ren, E. Cloutman-Green, M. Edirisinghe, L. Ciric, *Mater. Sci. Eng. C* **2017**, *74*, 315.
[63] X. Wu, S. Mahalingam, S. K. VanOosten, C. Wisdom, C. Tamerler, M. Edirisinghe, *Macromol. Biosci.* **2017**, *17*, 1.
[64] X. Hu, S. Liu, G. Zhou, Y. Huang, Z. Xie, X. Jing, *J. Control. Release* **2014**, *185*, 12.
[65] H. S. Yoo, T. G. Kim, T. G. Park, *Adv. Drug. Deliv. Rev.* **2009**, *61*, 1033.
[66] J. Zeng, L. Yang, Q. Liang, X. Zhang, H. Guan, X. Xu, X. Chen, X. Jing, *J. Control. Release* **2005**, *105*, 43.
[67] A. S. Perera, S. Zhang, S. Homer-Vanniasinkam, M.-O. Coppens, M. Edirisinghe, *ACS Appl. Mater. Interfaces* **2018**, *10*, 15524.
[68] H. D. Williams, N. L. Trevaskis, S. A. Charman, R. M. Shanker, W. N. Charman, C. W. Pouton, C. J. H. Porter, *Pharmacol. Rev.* **2013**, *65*, 315.
[69] R. Laitinen, K. Löbmann, C. J. Strachan, H. Grohganz, T. Rades, *Int. J. Pharm.* **2013**, *453*, 65.
[70] Y. Huang, W.-G. Dai, *Acta Pharm. Sin. B* **2014**, *4*, 18.
[71] W. Utembe, K. Potgieter, A. B. Stefaniak, M. Gulumian, *Part. Fibre Toxicol.* **2015**, *12*, 11.
[72] N. Bhardwaj, S. C. Kundu, *Biotechnol. Adv.* **2010**, *28*, 325.
[73] P. Gupta, C. Elkins, T. E. Long, G. L. Wilkes, *Polymer* **2005**, *46*, 4799.
[74] H. Fong, I. Chun, D. H. Reneker, *Polymer* **1999**, *40*, 4585.
[75] D. S. Katti, K. W. Robinson, F. K. Ko, C. T. Laurencin, *J. Biomed. Mater. Res. Part B Appl. Biomater.* **2004**, *70*, 286.
[76] M. Boegh, C. Foged, A. Müllertz, H. Mørck Nielsen, *J. Drug Delivery Sci. Technol.* **2013**, *23*, 383.
[77] F. Brako, R. Thorogate, S. Mahalingam, B. Raimi-Abraham, D. Q. M. Craig, ACS Applied Materials & Interfaces **2018**, *10*, 13381.
[78] F. Brako, B. T. Raimi-Abraham, S. Mahalingam, D. Q. M. Craig, M. Edirisinghe, *Int. J. Pharm.* **2018**, *540*, 31.
[79] J. Ahmed, R. K. Matharu, T. Shams, U. E. Illangakoon, M. Edirisinghe, *Macromol. Mater. Eng.* **2018**, 1700577.
[80] F. Khan, Y. Dahman, *Des. Monomers Polym.* **2012**, *15*, 1.
[81] D. C. Surrao, S. D. Waldman, B. G. Amsden, *Acta Biomater.* **2012**, *8*, 3997.
[82] D. Sankar, K. T. Shalumon, K. P. Chennazhi, D. Menon, R. Jayakumar, *Tissue Eng. Part A* **2014**, *20*, 1689.
[83] L. Matlock-Colangelo, A. J. Baeumner, *Lab Chip* **2012**, *12*, 2612.
[84] J. Shin, S.-J. Choi, I. Lee, D.-Y. Youn, C. O. Park, J.-H. Lee, H. L. Tuller, I.-D. Kim, *Adv. Funct. Mater.* **2013**, *23*, 2357.
[85] V. Vamvakaki, K. Tsagaraki, N. Chaniotakis, *Anal. Chem.* **2006**, *78*, 5538.
[86] D. He, B. Hu, Q. F. Yao, K. Wang, S. H. Yu, *ACS Nano* **2009**, *3*, 3993.
[87] K. Hettiarachchi, A. P. Lee, *J. Colloid. Interface Sci.* **2010**, *344*, 521.
[88] J. R. Lindner, *Nat. Rev. Drug Discovery* **2004**, *3*, 527.
[89] J. M. Tsutsui, F. Xie, R. T. Porter, *Cardiovasc. Ultrasound* **2004**, *2*, 23.
[90] E. M. Ahmed, *J. Adv. Res.* **2015**, *6*, 105.
[91] K. Kabiri, H. Omidian, M. J. Zohuriaan-Mehr, S. Doroudiani, *Polym. Compos.* **2010**, *32*, 277.
[92] N. Bhattarai, J. Gunn, M. Zhang, *Adv. Drug. Deliv. Rev.* **2010**, *62*, 83.
[93] J. Maitra, V. K. Shukla, *Am. J. Polym. Sci.* **2014**, *4*, 25.
[94] H. J. Kong, E. Wong, D. J. Mooney, *Macromolecules* **2003**, *36*, 4582.
[95] X. Su, S. Mahalingam, M. Edirisinghe, B. Chen, *ACS Appl. Mater. Interfaces* **2017**, *9*, 22223.
[96] K. Haraguchi, T. Takehisa, *Adv. Mater.* **2002**, *14*, 1120.
[97] E. Stojanovska, E. Canbay, E. S. Pampal, M. D. Calisir, O. Agma, Y. Polat, R. Simsek, N. A. S. Gundogdu, Y. Akgul, A. Kilic, *RSC Advances* **2016**, *6*, 83783.
[98] K. Yoon, K. Kim, X. Wang, D. Fang, B. S. Hsiao, B. Chu, *Polymer* **2006**, *47*, 2434.
[99] X. Tao, G. Zhou, X. Zhuang, B. Cheng, X. Li, H. Li, *RSC Adv.* **2015**, *5*, 5801.
[100] H. Bagheri, S. Asgari, H. Piri-Moghadam, *Chromatographia* **2014**, *77*, 723.
[101] B. Maddah, S. S. Javadi, A. Mirzaei, M. Rahimi-Nasrabadi, *J. Liq. Chromatogr. Related Technol.* **2015**, *38*, 208.
[102] M. L. Mejía, J. Zapata, D. P. Cuesta, I. C. Ortiz, L. E. Botero, B. J. Galeano, N. J. Escobar, L. M. Hoyos, *Revista Ingeniería Biomédica* **2017**, *11*, 13.
[103] Y.-K. Cheong, J. Calvo-Castro, L. Ciric, M. Edirisinghe, E. Cloutman-Green, U. E. Illangakoon, Q. Kang, S. Mahalingam, R. K. Matharu, R. M. Wilson, G. Ren, *Nanomaterials* **2017**, *7*, 152.
[104] L. Ciric, M. S. M. Brouwer, P. Mullany, A. P. Roberts, *FEMS Microbiol. Lett.* **2014**, *353*, 106.
[105] R. K. Matharu, Z. Charani, L. Ciric, E. Illangakoon Upulitha, M. Edirisinghe, *J. Appl. Polym. Sci.* **2018**, *0*, 46368.
[106] I. Sondi, B. Salopek-Sondi, *J. Colloid Interface Sci.* **2004**, *275*, 177.
[107] R. K. Matharu, H. Porwal, L. Ciric, M. Edirisinghe, *Interface Focus* **2018**, *8*, 20170058.
[108] E. Altun, O. A. Mehmet, F. Koc, M. Crabbe-Mann, F. Brako, R. Kaur-Matharu, G. Ozen, E. K. Serap, U. Edirisinghe, O. Gunduz, M. Edirisinghe, *Macromol. Mater. Eng.* **2018**, *303*, 1700607.
[109] P. Chawla, I. Bajaj, S. Survase, R. S. Singhal, *Food Technol. Biotechnol.* **2009**, *47*, 107.
[110] W. Czaja, A. Krystynowicz, S. Bielecki, R. M. Brown, Jr., *Biomaterials* **2006**, *27*, 145.
[111] E. Yang, J. Shi, Y. Xue, *J. Appl. Polym. Sci.* **2010**, *116*, 3688.
[112] L. Persano, A. Camposeo, C. Tekmen, D. Pisignano, *Macromol. Mater. Eng.* **2013**, *298*, 504.